Direct measurement via cyclotron resonance of the carrier effective masses in pristine diamond

Nobuko Naka,[1] Katsuyuki Fukai,[2] Yushi Handa,[2] and Ikuko Akimoto[2]
[1]*Department of Physics, Kyoto University, Kitshirakawa-Oiwake-cho, Sakyo-ku, Kyoto 606-8502, Japan*
[2]*Department of Materials Science and Chemistry, Wakayama University, Wakayama 640-8510, Japan*
(Received 16 April 2013; revised manuscript received 17 May 2013; published 26 July 2013)

We have determined effective mass parameters for ultrapure diamond by time-resolved cyclotron resonance of optically excited carriers. The transverse and longitudinal electron masses are found to be $m_t/m_0 = 0.280(2)$ and $m_l/m_0 = 1.56(2)$, where m_0 is the free-electron mass. The Luttinger parameters are extracted as $\gamma_1 = 2.67(2)$, $\gamma_2 = -0.40(2)$, and $\gamma_3 = 0.68(2)$, which give the light- and heavy-hole bands with considerable anisotropy and the split-off hole mass. The resonance widths indicate scattering times longer than 100 ps and carrier mobilities as high as 10^6 cm^2 V^{-1} s^{-1} at 10 K.

DOI: 10.1103/PhysRevB.88.035205 PACS number(s): 76.40.+b, 71.20.−b, 71.35.Gg

I. INTRODUCTION

Among various solid materials, diamond possesses fascinating properties; the high thermal conductivity, mechanical hardness, chemical stability, and the long spin coherence of a localized electron as a qubit are just some examples.[1] The crystal structure is isomorphic to those of silicon and germanium, and the constituent carbon atoms are lightest among the group-IV elements with the highest natural abundance of the isotope with zero nuclear spin. This provides a simple and ideal platform for state-of-the-art calculations for transport,[2,3] elastic,[4] optical and electronic structural[5] properties, etc. To our surprise, there is no direct measurement of the effective masses of photoexcited carriers in nondoped diamond despite the widespread interest. Therefore, the effective masses in diamond still come up for discussions in $\mathbf{k}\cdot\mathbf{p}$ perturbation theory[6,7] or in first-principles calculations.[8] The effective masses are related to the high carrier mobilities[9,10] in diamond, which determine the functionality in high-power electronics applications. In addition, photoexcited carriers in diamond form a scientifically rich many-body system. However, due to the lack of clear experimental determination, different effective-mass parameters have been used[11–13] in the arguments on the phase boundary for metal-insulator phase transitions involving condensation of electron-hole bound pairs (i.e., excitons) into an electron-hole liquid state as well as in the estimation of their binding energies.

In this paper, we present the cyclotron resonance (CR) of optically excited carriers in pristine diamond. This is realized by combining our laser spectroscopy technique with the nanosecond CR method that was recently developed for semiconductors with long carrier lifetimes[14] where the free carriers are produced by two-body collisions of excitons [see Fig. 1(a)]. In ultrapure diamond with less than 5-ppb (ppb denotes 10^{-9}) nitrogen and 1-ppb boron, we successfully obtained CR signals originated from free electrons and free holes [Fig. 1(b)]. We observe the largest effective masses and estimate the highest mobilities in diamond among group-IV elemental semiconductors. This means that an extremely long scattering time is achieved in diamond. The valence-band parameters, which describe the energy dispersions of the three hole bands, are extracted with high accuracy, and the results imply the necessity for including spin-orbit coupling for the valence bands.

Two reasons prevent a simple approach to determine the intrinsic material parameters for diamond. The first one is the unavailability of high-purity diamond crystals. In the 1960s, Rauch carried out a CR measurement at 70 GHz with a natural p-type diamond cooled at 4 K, which might be influenced by the existence of impurities.[15] In order to get rid of impurity transitions, Kono *et al.* applied a large magnetic field up to 150 T and measured the CR of thermally excited carriers at room temperature.[16] Other methods capable of extracting effective masses are mobility measurements by which only angle-averaged masses are obtained or spectroscopic analysis on shallow impurity levels according to the spherical effective-mass approach.[17] Since most of the semiconducting diamond is p type, information on the electron effective mass is sparse, and experimental values for the holes significantly scatter depending on the methods for measurements and analyses.

Second, diamond has an indirect energy gap of 5.49 eV in the deep ultraviolet region. The lack of suitable light sources for the photoexcitation of carriers had been making the measurements difficult. We have developed an efficient way to create photocarriers in diamond by using linear and nonlinear optical processes.[18] Now, we are able to generate free carriers in diamond with controlled spatial distribution at an arbitrary density and temperature by selecting the wavelength for optical excitation.[19] Also, the advancement of the crystal-growth technique by the chemical vapor deposition (CVD) method helps us to realize the CR study of optically excited long-life carriers in pristine diamond.

II. EXPERIMENTS

We used a single-crystal CVD diamond supplied by Element Six. A microwave of 0.1 mW at a frequency of $\nu = 9.64$ GHz irradiated the sample mounted in a dielectric cavity (MD5W1, Bruker) at $T = 10$ K under an external magnetic field.[20] Thus, the condition $h\nu < k_B T$ for the classical treatment[21] is satisfied. The temporal change in both real and imaginary parts of the microwave electric field was measured at a quadrature detector.[20] The light source was 5-ns pulses from an optical parametric oscillator (MOPO, Spectra-Physics) pumped by a Nd:YAG laser. We selected the excitation wavelength at 223.7 nm (i.e., photon energy of 5.541 eV) for which the penetration depth was $\sim$0.22 mm.[19]

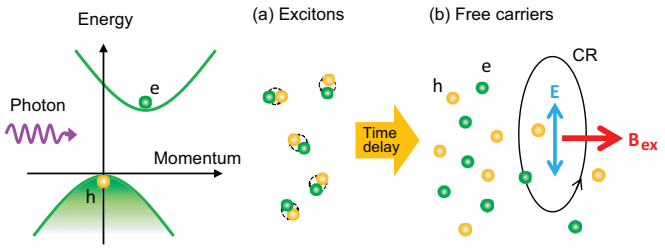

FIG. 1. (Color online) Concept of the time-resolved cyclotron resonance of optically excited carriers. We first generate excitons with optical pump below the band gap [panel (a)]. The excitons collide with each other and ionize into free carriers. The free carriers exhibit absorption of the microwave with the electric field **E** due to the CR motion in the plane perpendicular to the external magnetic field $\mathbf{B}_{ex}$ [panel (b)].

With the photon energy close to the indirect energy gap of diamond, excitons are generated via the phonon-assisted photoabsorption process. The initial density of the excitons is high enough that two excitons collide to ionize one into the free-carrier state against the exciton binding energy of 80 meV with the other nonradiatively recombining. This is the so-called Auger recombination process. The sole contribution of the free carriers to the CR signals is confirmed by our previous experiments on a semiconductor Cu_2O, which has an even larger exciton binding energy of 150 meV. All of the features: The quadratic increase in the CR signal intensity versus incident photon flux,[22] the CR transients changing with the density,[20,22] and the CR excitation spectra resonant to both one-photon[14] and two-photon[22] excitonic transitions, guarantee the free-carrier generation by two-body collisions. The long-wavelength excitation of excitons in diamond, rather than band-to-band excitation of free carriers, leads to deeper distribution of the carriers into the sample depth. Therefore, the carriers produced by excitonic collisions respond to the electric field of the microwave more sensitively.[20]

III. RESULTS AND DISCUSSION

Figures 2(a) and 2(b) show real and imaginary parts of the microwave absorption due to the cyclotron motion of the free carriers. The magnetic field forms an angle of 40° to the crystal axis of [001] in the $(1\bar{1}0)$ plane. The open circles in the inset show the temporal change in the position of the first peak (marked by lh), whose value has been converted to the effective mass. We observed a plasma shift[14] in the effective mass due to high-density carriers for the delay time shorter than 700 ns. On one hand, the transients decayed with a time constant ranging from 250 to 500 ns, depending on the excitation conditions slightly changed at different crystal orientations. In order to extract the effective masses free from the plasma shifts with a sufficiently good signal-to-noise ratio, the timing window of 800 ± 100 ns was selected for the resonance curves used for the analysis. The inverse scattering time can be obtained based on the resonance width as a function of delay time as indicated by the solid dots in the inset. We will discuss more details later in connection with the argument of mobility.

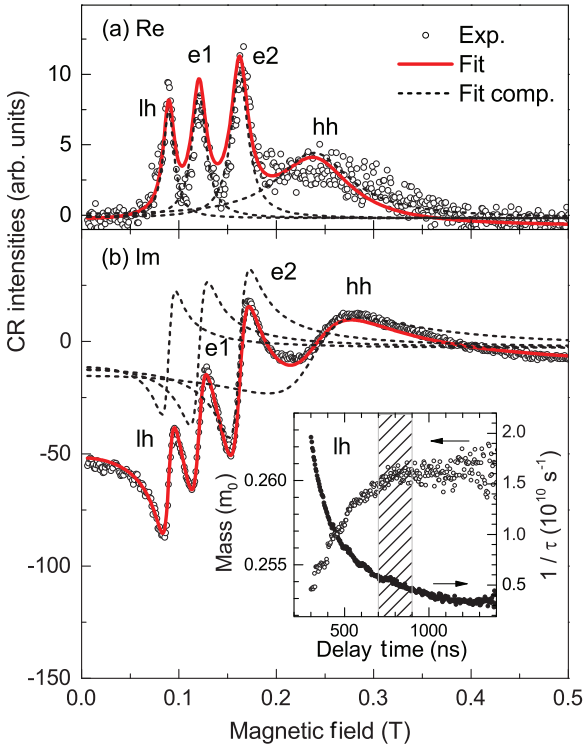

FIG. 2. (Color online) Cyclotron resonance curves in diamond at 10 K with the magnetic field applied along the direction of 40° to the [001] axis in the $(1\bar{1}0)$ plane. (a) Real and (b) imaginary parts of the microwave electric field are shown. Inset: The effective mass $m_{\rm eff} = eB_i/(2\pi\nu)$ and the inverse scattering time $1/\tau = 2\pi\nu\Gamma_i/B_i$ for the light hole as a function of delay time following the optical excitation. The hatched area indicates the timing window for the profiles in (a) and (b).

In the figure, four peaks are clearly seen. We fit the curves with the real and imaginary parts of the complex conductivity:[21] $(1 - iB_i/\Gamma_i)/\{(1 - iB_i/\Gamma_i)^2 + B_{ex}^2/\Gamma_i^2\}$. Here, the peak positions B_i and the linewidth Γ_i of the resonance are varied as the fitting parameters, and B_{ex} is the magnitude of the external magnetic field. The red solid lines represent the best fits with the sum of four components ($i = 1,2,3,4$), whereas, the dashed lines represent each resonance. B_i gives an effective mass by a relation $m_{\rm eff} = eB_i/(2\pi\nu)$, where e is the electric charge. Γ_i together with B_i gives a scattering time $\tau = B_i/(2\pi\nu\Gamma_i)$. Note that the real part is the power absorption, which is normally recorded in standard CR measurements.

Similar measurements and analysis were performed for different field directions as realized by rotating the sample around the [100] or $[1\bar{1}0]$ axis. A series of the data for the latter case is shown in Figs. 3(a) and 3(b). The conduction-band minimum in diamond is located along the [100] directions at ~76% of the X points of the Brillouin zone as inferred from optical spectra[23] or as predicted by band calculations.[7,24] Therefore, the electrons occupy the six conduction valleys at the Δ points. We assigned two peaks in Figs. 3(a) and 3(b) to be due to electrons in inequivalent conduction valleys and the other two peaks to light and heavy holes as indicated by e1, e2, lh, and hh, respectively.

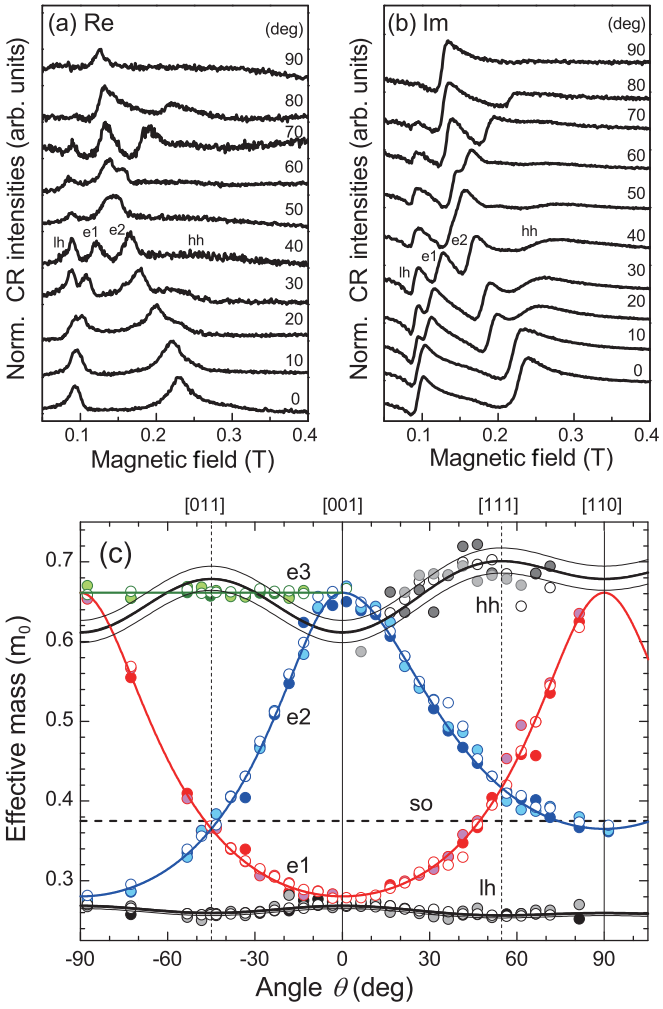

FIG. 3. (Color online) (a) Real and (b) imaginary parts of the cyclotron resonance curves at different field directions measured from the [001] axis. (c) Angular dependence of the effective masses of e1, e2, e3, lh, and hh. The circles are data points, and the solid lines are fits as explained in the text. The dashed horizontal line labeled "so" indicates the calculated split-off hole mass. The thin black lines represent deviations in the calculated hole masses due to errors in A, B', and C. The negative angles mean the magnetic field in the (100) plane and the positive angles in the $(1\bar{1}0)$ plane.

Figure 3(c) shows the angular dependence of the effective masses. The solid circles are obtained by simultaneous fits of the real and imaginary parts. The shaded (open) circles are obtained by fitting solely with a real (imaginary) part. In this figure, the results from the two runs of experiments for different orientations of the rotation axis are combined. Namely, the negative angles mean the magnetic field in the (100) plane for the rotation axis along [100], whereas, the positive angles mean the magnetic field in the $(1\bar{1}0)$ plane for the rotation axis along $[1\bar{1}0]$. The electron peaks e1 and e2 originate from two- and four-equivalent valleys, respectively, for the magnetic field in the $(1\bar{1}0)$ plane. On the other hand, they split into three peaks with each for two-equivalent valleys for the field in the (100) plane. We refer to the third one as e3. We found a strong angular dependence of the masses except for e3. For e3 the long axis of the ellipsoidal energy surface forms a right angle with the field, thus, giving the angle-independent effective mass.

TABLE I. Comparison of the electron and hole masses and the mass anisotropy a, defined in the text in diamond (columns a–d), silicon,[21] and germanium[21] by experiment and theory. a: Present work with errors in parentheses; b: theory including spin-orbit interaction;[7] c: theory without spin-orbit interaction (*: geometrical average);[7] and d: experiment based on the acceptor levels.[25] All masses are in units of the free-electron mass.

	a	b	c	d	Si	Ge
m_t	0.280(2)	0.341	0.341		0.19	0.082
m_l	1.56(2)	1.50	1.50		0.97	1.58
m_{lh}	0.260(2)	0.284	0.471*	0.28	0.146	0.043
m_{hh}	0.67(2)	0.643	0.798*	1.20	0.520	0.336
m_{lh}^{111}	0.248(2)	0.264	0.778	0.25	0.152	0.042
m_{lh}^{100}	0.288(4)	0.366	0.366	0.41	0.175	0.046
m_{lh}^{110}	0.255(2)	0.276	0.366	0.27	0.156	0.043
m_{hh}^{111}	0.76(2)	0.778	0.778	2.22	0.620	0.436
m_{hh}^{100}	0.54(2)	0.427	0.366	0.51	0.400	0.244
m_{hh}^{110}	0.70(2)	0.690	1.783	1.47	0.555	0.368
a_{lh}	−0.14	−0.28	+1.13	−0.39	−0.13	−0.08
a_{hh}	+0.42	+0.82	+1.13	+3.35	+0.55	+0.79
m_{so}	0.375(8)	0.394	0.278*	0.457	0.25	0.08

For the magnetic field applied at a polar angle θ from the [001] axis, the electron masses are given by[21]

$$m_{ei}(\theta) = \left[\frac{m_t^2 m_l}{m_t[1-g_i(\theta)^2] + m_l g_i(\theta)^2}\right]^{1/2}. \quad (1)$$

Here, $g_1(\theta) = \pm\cos\theta$ and $g_2(\theta) = \pm\sin\theta/\sqrt{2}$ for the magnetic field in the $(1\bar{1}0)$ plane, and $g_1(\theta) = \pm\cos\theta$, $g_2(\theta) = \pm\sin\theta$, and $g_3(\theta) = 0$ for that in the (100) plane. We obtained the transverse electron effective mass $m_t/m_0 = 0.2804(15)$ and the longitudinal one $m_l/m_0 = 1.560(17)$ from the best fit, where m_0 is the free-electron mass. This means that the electrons are in highly asymmetric valleys along the [001] directions with the mass anisotropy factor of $m_l/m_t = 5.56$. Nava *et al.*[9] extracted electron effective masses using the transport theory based on the measured drift mobility. Their values ($m_t/m_0 = 0.36$ and $m_l/m_0 = 1.4$) are not far from ours if we consider the uncertainty of about 10% in their simulation results. Theoretical values[7] are also in reasonable agreement with ours as listed in columns b and c in Table I.

On the other hand, the doubly degenerate valence-band maximum is located at the zone center, that is, the Γ point. The light- and heavy-hole (lh, hh) bands are warped by the band mixing and are expressed as $E_{hh,lh}(\mathbf{k}) = A\mathbf{k}^2 \pm [B^2\mathbf{k}^4 + C^2(k_x^2k_y^2 + k_y^2k_z^2 + k_z^2k_x^2)]^{1/2}$, where $\mathbf{k} = (k_x, k_y, k_z)$ is the wave vector. The anisotropic mass can be approximated as[21]

$$m_{hh,lh}(\theta) = -\frac{1}{A \pm B'}\left[1 \pm \frac{C^2 f(\theta)}{16B'(A \pm B')}\right], \quad (2)$$

where $B'^2 = B^2 + C^2/4$ and the angular dependence is given by $f(\theta) = (1-3\cos^2\theta)^2/4$ for the field in the $(1\bar{1}0)$ plane and $f(\theta) = 1-3\cos^2\theta\sin^2\theta$ for that in the (100) plane. We consider that the data points for the light hole are more reliable than those for the heavy hole which have a wider resonance peak. Therefore, we first performed a

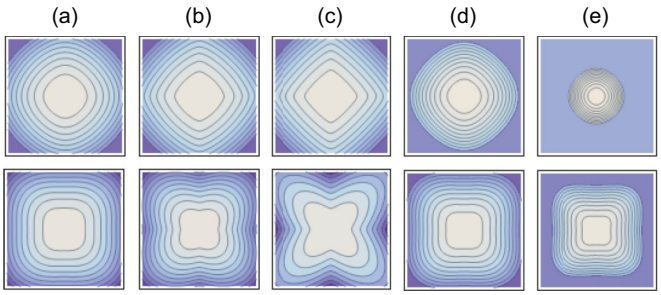

FIG. 4. (Color online) Comparison of the energy dispersions around the Γ point within the ±2% of the Brillouin zone of diamond for the light hole (upper panels) and the heavy hole (lower panels) in the k_x-k_y plane. (a) Present study for diamond, (b) theory with spin-orbit coupling for diamond,[7] (c) previous experiment for diamond,[25] (d) silicon,[21] and (e) germanium.[21] The contours represent light-hole energies from −0.6 to −6 meV in steps of −0.6 meV and heavy-hole energies from −0.3 to −3 meV in steps of −0.3 meV.

fit with the light-hole mass and then confirmed that the heavy-hole mass is reproduced by Eq. (2) with the common parameters as for the light hole. We find the parameters for the best fit: $A = -2.670(20)$; $B' = 1.245(25)$; $|C| = 1.898(48)$ in units of $\hbar^2/(2m_0)$. Using these parameters, we calculated angle-averaged hole masses: $m_{lh}/m_0 = 2/\hbar^2/[-A + (B^2 + C^2/5)^{1/2}] = 0.2604(23)$ and $m_{hh}/m_0 = 2/\hbar^2/[-A - (B^2 + C^2/5)^{1/2}] = 0.667(15)$, which can be compared with $m_{lh}/m_0 = 0.3$ and $m_{hh}/m_0 = 1.1$ by Reggiani *et al.*[10] and $m(2)/m_0 = 0.31$ and $m(3)/m_0 = 0.70$ by Kono *et al.*[16]

The corresponding Luttinger parameters are $\gamma_1 = -(2m_0/\hbar^2)A = 2.670(20)$, $\gamma_2 = -(m_0/\hbar^2)B = -0.403(24)$, and $\gamma_3 = (m_0/\hbar^2)(B^2 + C^2/3)^{1/2} = 0.680(18)$ where we take a positive value for B considering that the Γ_2^- band is located higher than the Γ_4^- band at the zone center.[7] In Table I, we summarized the hole masses for different **k** directions in the present paper in comparison with theoretical values. The mass anisotropy defined by $a = (m^{111} - m^{100})/m^{100}$ is also given, where m^{ijk} denotes the mass value for **k** along the $[ijk]$ direction. Column b gives the values by $\mathbf{k}\cdot\mathbf{p}$ theory including spin-orbit interaction with $\gamma_1 = 2.54$, $\gamma_2 = -0.10$, $\gamma_3 = 0.63$, and column c without spin-orbit interaction.[7] At least to reproduce the signs of the a's, inclusion of the spin-orbit coupling is necessary. Column d shows the experimental values of Bashenov *et al.*[25] that are extracted based on the accepter levels. Other experimental values are very different from ours as described in Ref. 7. To visualize the differences corresponding to columns a, b, and d, we plotted the hole-band dispersions in Figs. 4(a)–4(c). The upper panels are contour plots of the light-hole energy in the k_x-k_y plane. The present result (a) shows the most rounded diamond shape, indicating the small negative anisotropy for the light hole. The lower panels are similar plots for the heavy hole. The squarelike contours in (a) are originated from the positive anisotropy.

In Table I, we also listed the mass parameters for other diamond-structure materials. For silicon and germanium, the conduction-band minimum is located at the Δ and the L points, respectively, whereas, the valence-band maximum is at the Γ point for both. The angle-averaged masses are largest in diamond among the three materials. On the other hand, the hole mass anisotropy in diamond is similar to that in silicon. This situation can be seen by comparing Fig. 4(a) for diamond with Fig. 4(d) for silicon and Fig. 4(e) for germanium. The similarity stems from the fact that the Kane energy[6] roughly scales as the inversely squared lattice constant and cancels out with the large direct band gap ($E_0 = 7.3$ eV) of diamond.

The spin-orbit splitting in diamond is considered to be $\Delta = 6$ meV,[15] that is much smaller than those in other semiconductors. Experimentally, we did not find any systematic peak due to the split-off hole. The reason is that the relaxation from the split-off to the heavy- or light-hole bands occurs faster[19] than the present temporal resolution of 15 ns. However, the small spin-orbit coupling ($\Delta \ll E_0$) simplifies the expression for the split-off hole mass[6] so that we get $m_{so}/m_0 \approx 1/\gamma_1 = 0.375(8)$. Again, comparison of our result with theories clearly indicates the importance of the inclusion of the spin-orbit coupling. Given the three hole mass values, we can define the exciton masses: the center-of-motion mass $M_{ex}/m_0 = 0.760$ and the electron-hole reduced mass $\mu_{ex}/m_0 = 0.189$. This leads to about a −14% correction to the values used earlier[11–13] and very recently[26] concerning the electron-hole liquid state.

From the observed resonance widths at 10 K, we obtained scattering rates on the order of 10^{10} s^{-1} (see the inset of Fig. 2). The corresponding scattering times are a few hundred picoseconds, and the mobilities are $\mu_e = 2 \times 10^6$ cm^2 V^{-1} s^{-1} for electrons and $\mu_h = 9 \times 10^5$ cm^2 V^{-1} s^{-1} for holes. In diamond, the dominant scattering occurs with acoustic phonons, and the rate scales as $T^{3/2}$,[27] where T is the temperature. In practice, we observed broadening of the CR peaks up to 30 K, and extrapolation at room temperature gives $\mu_e = 10\,000$ and $\mu_h = 6000$ cm^2 V^{-1} s^{-1}. These values are higher than the values $\mu_{e(h)} = 1500$ (450) cm^2 V^{-1} s^{-1} for silicon,[28] $\mu_{e(h)} = 3900$ (1900) cm^2 V^{-1} s^{-1} for germanium,[28] and for diamond as reported in Ref. 27. Recently, the parameter-free first-principles theory on group-IV semiconductors[29] predicted the spin-relaxation time for the conduction electrons in diamond due to phonon scattering. On the other hand, measurements of the spin-relaxation time of conduction electrons in pristine diamond are still beyond the experimental reach. More detailed measurements on the temperature dependence by using our method would give a clue clarifying the relaxation mechanism of conduction electrons in the near future.

IV. CONCLUSION

We have directly measured the effective masses of electrons and light (heavy) holes within 1 (2.4)% accuracy in pristine diamond under optical excitation. We figured out the large electron mass with asymmetric valley structure, the oppositely warped light- and heavy-hole bands, as well as the high mobilities that can exceed the previous records. The long scattering times in our ultrapure samples allowed us to use the low-frequency microwave, which was suited to probe the warping of the hole bands affected by the band mixing. Our complete data set, including the split-off hole mass, stimulates further improvement of the band calculations with the inclusion of spin-orbit coupling.

ACKNOWLEDGMENTS

This work was partially supported by a Grant-in-Aid for Scientific Research on Innovative Areas "DYCE" (Grants No. 20104002 and No. 23104720) of MEXT, Japan and by the Asahi Glass Foundation. N.N. thanks N. Mizuochi (Osaka University) for the useful discussion on the sample quality.

[1] I. Aharonovich, A. D. Greentree, and S. Prawer, Nat. Photonics **5**, 397 (2011).
[2] D. A. Broido, L. Lindsay, and A. Ward, Phys. Rev. B **86**, 115203 (2012).
[3] H. Lofas, A. Grigoriev, J. Isberg, and R. Ahuja, Appl. Phys. Lett. **102**, 092106 (2013).
[4] M. N. Valdez, K. Umemoto, and R. M. Wentzcovitch, Appl. Phys. Lett. **101**, 171902 (2012).
[5] F. Giustino, S. G. Louie, and M. L. Cohen, Phys. Rev. Lett. **105**, 265501 (2010).
[6] P. Lawaetz, Phys. Rev. B **4**, 3460 (1971).
[7] M. Willatzen, M. Cardona, and N. E. Christensen, Phys. Rev. B **50**, 18054 (1994).
[8] H. Lofas, A. Grigoriev, J. Isberg, and R. Ahuja, AIP Adv. **1**, 032129 (2011).
[9] F. Nava, C. Canali, C. Jacobini, and L. Reffiani, Solid State Commun. **33**, 475 (1980).
[10] L. Reggiani, S. Bori, C. Canali, and F. Nava, Solid State Commun. **30**, 333 (1979).
[11] R. Sauer, N. Teofilov, and K. Thonke, Diamond Relat. Mater. **13**, 691 (2004).
[12] R. Shimano, M. Nagai, K. Horiuch, and M. Kuwata-Gonokami, Phys. Rev. Lett. **88**, 057404 (2002).
[13] N. Naka, J. Omachi, and M. Kuwata-Gonokami, Phys. Rev. B **76**, 193202 (2007).
[14] N. Naka, I. Akimoto, M. Shirai, and K. Kan'no, Phys. Rev. B **85**, 035209 (2012).
[15] C. J. Rauch, Phys. Rev. Lett. **7**, 83 (1961).
[16] J. Kono, S. Takeyama, T. Takamasu, N. Miura, N. Fujimori, Y. Nishibayashi, T. Nakajima, and K. Tsuji, Phys. Rev. B **48**, 10917 (1993).
[17] A. Baldereschi and N. O. Lipari, Phys. Rev. B **8**, 2697 (1973).
[18] N. Naka, T. Kitamura, J. Omachi, and M. Kuwata-Gonokami, Phys. Status Solidi B **245**, 2676 (2008).
[19] Y. Hazama, N. Naka, M. Kuwata-Gonokami, and K. Tanaka (in preparation).
[20] I. Akimoto, S. Torai, N. Naka, and M. Shirai, Eur. Phys. J. B **85**, 374 (2012).
[21] G. Dresselhaus, A. F. Kip, and C. Kittel, Phys. Rev. **98**, 368 (1955).
[22] N. Naka, I. Akimoto, and M. Shirai, Phys. Status Solidi B (to be published) (2013).
[23] P. J. Dean, E. C. Lightowlers, and D. R. Wright, Phys. Rev. **140**, A352 (1965).
[24] W. Saslow, T. K. Bergstresser, and M. L. Cohen, Phys. Rev. Lett. **16**, 354 (1966).
[25] V. K. Bashenov, A. G. Gontar, and A. G. Petukhov, Phys. Status Solidi B **108**, K139 (1981).
[26] M. Kozak, F. Trojanek, T. Popelar, and P. Maly, Diamond Relat. Mater. **34**, 13 (2013).
[27] J. Isberg, J. Hammersberg, E. Johansson, T. Wikstrom, D. J. Twitchen, A. J. Whitehead, S. E. Coe, and G. A. Scarsbrook, Science **297**, 1670 (2002).
[28] S. M. Sze, *Physics of Semiconductor Devices* (Wiley Interscience, New York, 1981).
[29] O. D. Restrepo and W. Windl, Phys. Rev. Lett. **109**, 166604 (2012).